InGaN/GaN laser diode characterization and quantum well number effect

S. M. Thahab*, H. Abu Hassan, and Z. Hassan

Nano-Optoelectronics Research and Technology Laboratory, School of Physics, Universiti Sains Malaysia, 11800 Penang, Malaysia

**E-mail: sabahmr@yahoo.com*

Received September 12, 2008

The effect of quantum well number on the quantum efficiency and temperature characteristics of InGaN/GaN laser diodes (LDs) is determined and investigated. The 3-nm-thick $In_{0.13}Ga_{0.87}N$ wells and two 6-nm-thick GaN barriers are selected as an active region for Fabry-Perot (FP) cavity waveguide edge emitting LD. The internal quantum efficiency and internal optical loss coefficient are extracted through the simulation software for single, double, and triple InGaN/GaN quantum wells. The effects of device temperature on the laser threshold current, external differential quantum efficiency (DQE), and output wavelength are also investigated. The external quantum efficiency and characteristic temperature are improved significantly when the quantum well number is two. It is indicated that the laser structures with many quantum wells will suffer from the inhomogeneity of the carrier density within the quantum well itself which affects the LD performance.

OCIS codes: 140.0140, 270.0270, 140.2020.
doi: 10.3788/COL20090703.0226.

InGaN-based semiconductors have recently attracted much attention by the researchers, especially for their light-emitting device applications, such as high-brightness light-emitting diodes (LEDs) and continuous-wave (CW) multi quantum wells (MQWs) blue laser diodes (LDs). However, their optical properties are strongly affected by the quantum-confined Stark effect (QCSE) due to the presence of a large piezoelectric (PZ) field in the quantum well which arises from the strain caused by the lattice mismatch between GaN and InGaN[1,2].

The most important operating parameters in InGaN/GaN LDs are the internal quantum efficiency η_i, the internal loss α_i, and the transparency current density J_0[3,4]. The characteristic temperature is also a very important parameter from the viewpoint of the practical application of these lasers. The external differential quantum efficiency (DQE) η_d depends on η_i and the photon losses η_0 as[5]

$$\eta_d = \eta_i \eta_0. \quad (1)$$

η_0 can be expressed as

$$\eta_0 = \alpha_m / (\alpha_i + \alpha_m), \quad (2)$$

where α_m is the optical mirror loss coefficient:

$$\alpha_m = L^{-1} \ln(1/R), \quad (3)$$

which is depending on the laser length L and the reflectivity of mirror facets of the laser R, leading to the common expression of

$$\frac{1}{\eta_d} = \frac{1}{\eta_i}\left(\frac{L\alpha_i}{\ln(1/R)} + 1\right). \quad (4)$$

$\eta_d^{-1}(L)$ is widely used to determine η_i and α_i from the length-current (L-I) measurements with different laser lengths. The internal quantum efficiency is independent of the geometrical properties of the laser device, such as the cavity length or the stripe width. In this letter, we extract these parameters for InGaN/GaN LDs with various quantum well numbers. The effect of well number on the temperature characteristics is also investigated through the simulation software.

Experimental and theoretical work done by Domen *et al.*[6] concluded that the InGaN LD quantum efficiency could be improved when the number of wells is decreased. Our work supports the prior research result and explains the reasons behind it. Advanced laser simulation is used to analyze the internal physical processes of the InGaN/GaN LD. We have also utilized the commercially available laser simulation software[7] to reveal the performance limiting mechanisms and to explore the design optimization options.

The laser simulation program solved the Poisson equation, the current continuity equations, the photon rate equation, and the scalar wave equation by using the two-dimensional (2D) simulator. In addition, the carrier drift-diffusion model which includes Fermi statistics and incomplete ionization was included in our simulation models.

The Shockley Read-Hall (SRH) recombination lifetimes of electrons and holes are assumed to be 1 ns. However, this is a rough estimate since the type and density of recombination centers are sensitive to the technological process. From its bandgap dependence in other materials, a very small Auger parameter of $C = 1 \times 10^{-34}$ (cm^6/s) is estimated for GaN. Thus, even with large carrier densities, the Auger recombination in nitride materials is negligible. In our strained InGaN quantum wells, GaN values are used for the deformation potentials.

We started with a simple free carrier gain model including a hyperbolic-cosine broadening function with 0.1-ps scattering time. Optical reflection and waveguide mainly

1671-7694/2009/030226-05 © 2009 Chinese Optics Letters

depend on the refractive index profile inside the device. For photon energies close to the bandgap, the refractive index is a strong function of wavelength. The refractive indices of ternary alloys involved are extracted from GaN waveguide measurements[8,9] using bandgap variations ($x < 0.3$) and are given by

$$n(\mathrm{Al}_x\mathrm{Ga}_{1-x}\mathrm{N}) = 2.5067 - 0.43x, \quad (5)$$

$$n(\mathrm{In}_x\mathrm{Ga}_{1-x}\mathrm{N}) = 2.5067 + 0.91x. \quad (6)$$

The bandgap energies of the $\mathrm{In}_x\mathrm{Ga}_{1-x}\mathrm{N}$ and $\mathrm{Al}_x\mathrm{Ga}_{1-x}\mathrm{N}$ ternary alloys at room temperature are governed by

$$E_{\mathrm{gIn}_x\mathrm{Ga}_{1-x}\mathrm{N}} = xE_{\mathrm{gInN}} + (1-x)E_{\mathrm{gGaN}} - 1.43x(1-x), \quad (7)$$

$$E_{\mathrm{gAl}_x\mathrm{Ga}_{1-x}\mathrm{N}} = xE_{\mathrm{gAlN}} + (1-x)E_{\mathrm{gGaN}} - 1.3x(1-x), \quad (8)$$

E_{gInN}, E_{gGaN}, and E_{gAlN} are the bandgap energies of InN, GaN, and AlN at room temperature, respectively. The bandgap energies of InN, GaN, and AlN used in our simulation are 0.77, 3.42, and 6.2 eV, respectively[10,11].

The effective masses of electrons and holes for the active layer $\mathrm{In}_x\mathrm{Ga}_{1-x}\mathrm{N}$ used in our laser simulation were calculated by

$$m_{\mathrm{e,In}_x\mathrm{Ga}_{1-x}\mathrm{N}} = m_{\mathrm{e,GaN}} + x(m_{\mathrm{e,InN}} - m_{\mathrm{e,GaN}}), \quad (9)$$

$$m_{\mathrm{hh,In}_x\mathrm{Ga}_{1-x}\mathrm{N}} = m_{\mathrm{hh,GaN}} + x(m_{\mathrm{hh,InN}} - m_{\mathrm{hh,GaN}}), \quad (10)$$

$$m_{\mathrm{lh,In}_x\mathrm{Ga}_{1-x}\mathrm{N}} = m_{\mathrm{lh,GaN}} + x(m_{\mathrm{lh,InN}} - m_{\mathrm{lh,GaN}}), \quad (11)$$

where $m_{\mathrm{e,In}_x\mathrm{Ga}_{1-x}\mathrm{N}}$ is the effective mass of electrons in $\mathrm{In}_x\mathrm{Ga}_{1-x}\mathrm{N}$ material, $m_{\mathrm{hh,In}_x\mathrm{Ga}_{1-x}\mathrm{N}}$ and $m_{\mathrm{lh,In}_x\mathrm{Ga}_{1-x}\mathrm{N}}$ are the effective masses of heavy and light holes in $\mathrm{In}_x\mathrm{Ga}_{1-x}\mathrm{N}$, respectively. $m_{\mathrm{e,InN}}$ for InN is $0.1m_0$ and $m_{\mathrm{e,GaN}}$ for GaN is $0.151m_0$, while $m_{\mathrm{hh,InN}}$ and $m_{\mathrm{lh,InN}}$ of InN are $1.44m_0$ and $0.157m_0$ respectively, and $m_{\mathrm{hh,GaN}}$ and $m_{\mathrm{lh,GaN}}$ are $1.595m_0$ and $0.261m_0$, respectively[10], whereby m_0 is the electron mass in the free space.

A schematic diagram of the LD structure is shown in Fig. 1. A 3-μm n-type GaN layer is assumed to be grown firstly, then followed by a 0.4-μm n-type $\mathrm{Al}_{0.07}\mathrm{Ga}_{0.93}\mathrm{N}$ cladding layer and a 0.1-μm n-type GaN guiding layer. The active region of the preliminary LD structure under study consists of a 3-nm $\mathrm{In}_{0.13}\mathrm{Ga}_{0.87}\mathrm{N}$ well that is sandwiched between two 6-nm GaN barriers. A 0.02-μm p-$\mathrm{Al}_{0.15}\mathrm{Ga}_{0.85}\mathrm{N}$ stop layer is assumed to be grown on the top of the active region, followed by a 0.1-μm p-type GaN guiding layer, a 0.4-μm p-$\mathrm{Al}_{0.07}\mathrm{Ga}_{0.93}\mathrm{N}$ cladding layer, and a 0.1-μm p-GaN contact layer.

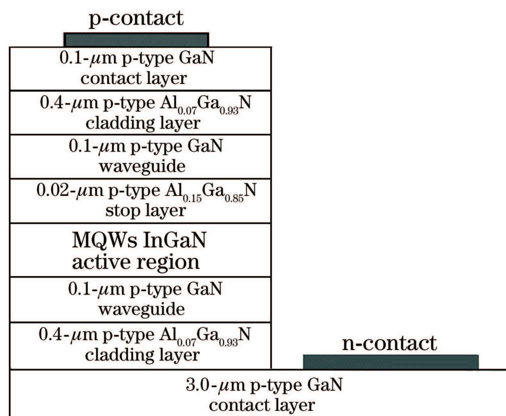

Fig. 1. Schematic diagram of the preliminary InGaN LD.

For our InGaN/GaN LD, the parameters including the output power, threshold current, slope efficiency, and external DQE as functions of the well number are shown in Fig. 2. A maximum output power of 16.6 mW and a lowest threshold current of 13.1 mA are obtained when the quantum well number is two. These results are in line with other experimental results obtained by many researchers[6,12]. For fewer quantum wells, the gain begins to be saturated before lasing is achieved. For more quantum wells, increasing the current is needed to pump the additional wells above transparency.

In addition, laser structures with many quantum wells also suffer from inhomogeneity of the carrier density within the quantum wells, as shown in Fig. 3. It is seen that as the number of quantum wells increases, the nonuniformity of carrier injection increases too. It is also observed that the carrier distributions are inhomogeneous and increasing towards the p-side in the laser structure. This is ascribed to the poor hole injection due to the low mobility and thermal velocity of the hole itself. Thus, the hole density becomes higher on the p-side and the electrons are attracted to the p-side.

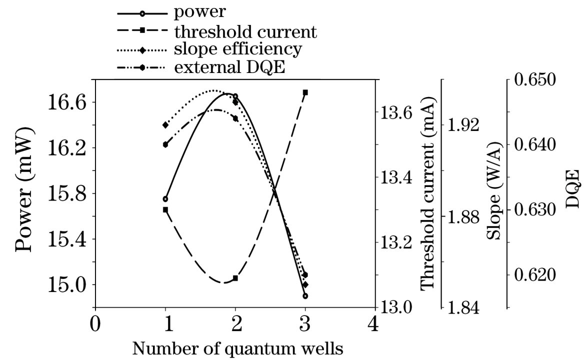

Fig. 2. Laser output power, slope efficiency, threshold current, and DQE as functions of well number of the MQWs InGaN LD. Cavity length $L = 800$ μm, width $W = 1$ μm, temperature $T = 300$ K.

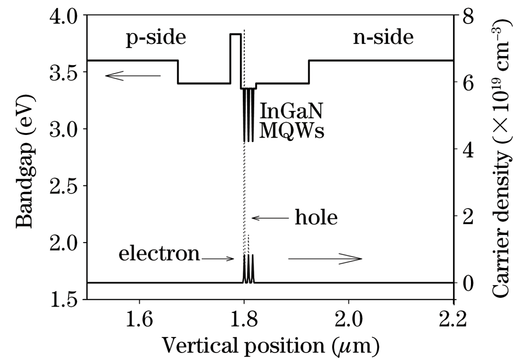

Fig. 3. Carrier density distribution profile in the InGaN MQWs LD.

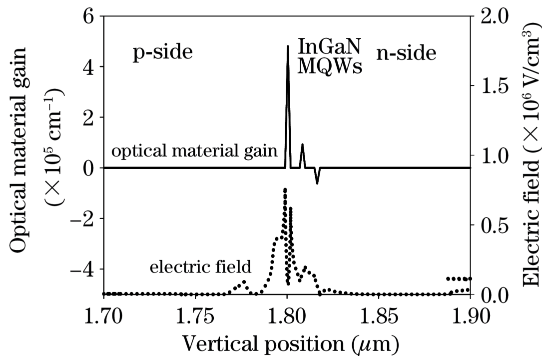

Fig. 4. Optical material gain and internal electric field in the InGaN LD.

The optical material gain inside the quantum wells is shown in Fig. 4. The quantum well in the left side (p-side) has a higher optical material gain due to the use of $Al_{0.15}Ga_{0.85}N$ blocking layer in the p-side of which the electrons tend to accumulate in the left quantum well. The holes are difficult to be moved from the left quantum well to the right quantum well due to the relatively large effective mass, low mobility, and high band offset in the valence band. Therefore, more holes are expected in the left quantum well. Since the left quantum well possesses more electrons and holes as compared with the right quantum well, it has higher population inversion and hence higher stimulated recombination rate.

It was also found that the optical gain is generated in the two wells on the p-side. No gain value was observed in the third well in the n-side and this layer acted as an absorption layer that increased the laser threshold current and suppressed the quantum efficiency. As a result, it decreased the laser output power. The internal field in InGaN quantum wells causes the separation of the electron and hole wave functions, thus reducing the wave function overlap integral.

Consequently, when the carrier lifetime increases, the oscillator strength reduces. As the carrier density in the quantum well increases, screening of the internal field occurs. Hence, a blue shift of the laser emission wavelength was observed in our LD, as shown in Fig. 5[13]. The presence of the built-in electric field modifies the electronic states in quantum wells and lowers the optical gain of the active region of the laser. The electrons and holes are, indeed, spatially separated by the polarization filed, but the free carrier induced field is opposite to the polarization field. The two fields tend to cancel each other out for higher sheet densities, thus re-establishing the conditions for the electron-hole recombination emission. The wavelength of the light emitted from LD quantum well depends not only on the bandgap, but also on the large internal electric field due to the PZ and spontaneous polarization. The PZ field arises from the strain due to the lattice mismatch between the InGaN well and the GaN barriers and causes the red shift in the optical transition energy.

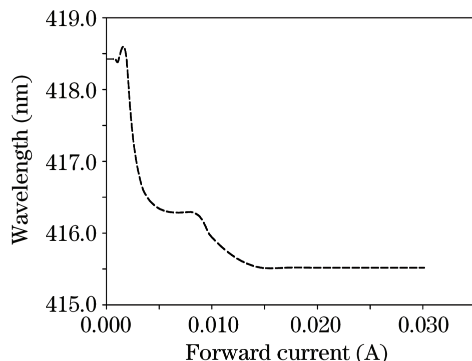

Fig. 5. Output wavelength of the DQW InGaN/GaN LD as a function of forward current.

Figure 6 shows the calculation method for the parameters of η_i and α_i with respect to the inverse value of DQE as a function to the cavity length. We obtained the values of 97% and 9.69 cm^{-1} of η_i and α_i respectively in the case of double-quantum-well (DQW) LD. The values of internal quantum efficiency η_i and internal loss α_i are a direct indication of the efficiency of our DQW InGaN LD. It can be seen that the value of the external DQE is smaller than the internal quantum efficiency, and this difference is related to the different internal loss mechanism in the LD device.

The transparency current J_0 is defined by the position of the quantum levels, the band structure parameters of the quantum level, and the band structure parameters of the strained material in the active region. In order to obtain J_0 value, we have plotted the curve of threshold current density versus the inverse cavity length, as shown in Fig. 7. The intercept of the linear fit line of the data plotted in this curve with the vertical axis provides us with the transparency threshold current density value. Then it is observed that the DQW has lower J_0 value compared with that in single-quantum-well (SQW) and triple-quantum-well (TQW), as shown in Fig. 8.

However, it is inexpedient to reduce the transparency current component by making the quantum well thinner

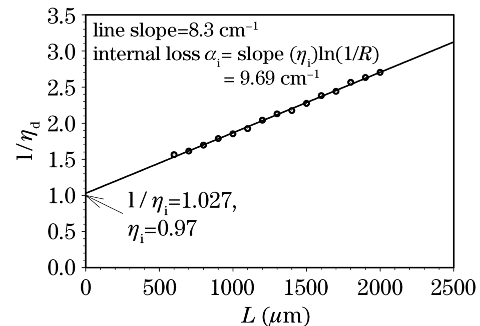

Fig. 6. Inverse of the external quantum efficiency $1/\eta_d$ as a function of cavity length L of the DQW InGaN LD.

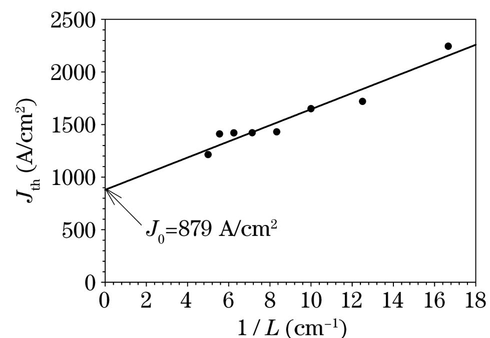

Fig. 7. Threshold current density J_{th} as a function of inverse of cavity length $1/L$ of the DQW InGaN LD at 300 K.

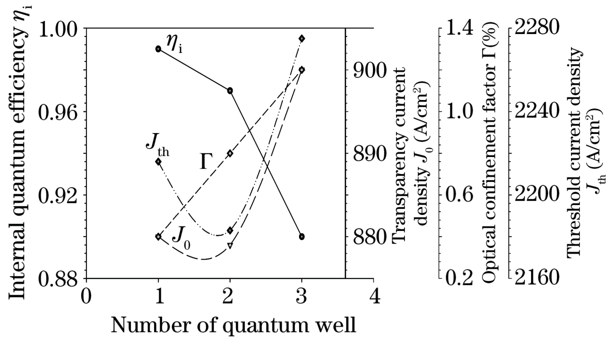

Fig. 8. Internal quantum efficiency, transparency current density, threshold current density, and confinement factor as functions of quantum well number of the MQW InGaN LD at room temperature. $L = 800$ μm, $W = 1$ μm.

because of the strong decrease in the optical confinement factor and the rise in the threshold current density. Our results suggested reducing this parameter by changing the laser quantum well number instead of changing the quantum well thickness. The LD applications require good thermal stability of the employed LDs in terms of wavelength emission and threshold current. The thermal sensitivity of the latter parameter is described by an exponential equation as

$$J_{\text{th}} = J_0 \exp(T/T_0), \quad (12)$$

where T_0 is the characteristic temperature that jointly represents the temperature dependence of various mechanisms such as optical gain, radiative and non-radiative recombinations, carrier escape, etc., which determine the value of the device threshold current. However, the increase in the threshold current of the LD with device temperature is ascribed to that more current is needed to achieve the necessary population inversion at higher temperature, while the center wavelength of a LD is directly proportional to its operating temperature. Figure 9 shows that as the temperature increases, the threshold current increases and the DQE decreases due to the increases in the internal losses and non-radiative recombinations in the laser active region. Additionally, a red shift was observed in the laser peak emission wavelength with the increase in temperature.

Regarding the characteristic temperature T_0 of the LD, it is commonly referred to be a measure of the temperature sensitivity of the device. Higher values of T_0 imply that the threshold current density increases and the

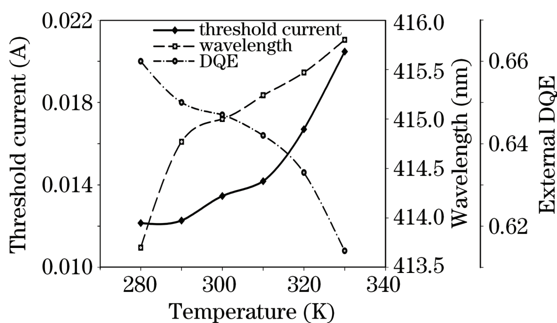

Fig. 9. Threshold current, peak wavelength, and DQE as functions of device temperature of the InGaN DQW LD.

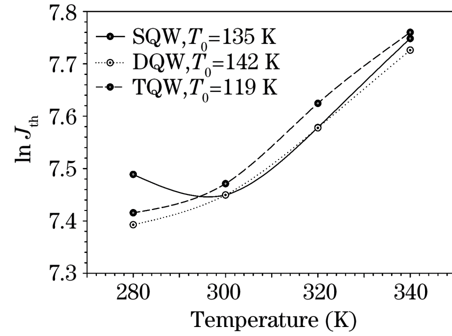

Fig. 10. Variations of the threshold current density ($\ln J_{\text{th}}$) with increasing temperature for SQW, DQW, and TQW InGaN LD.

external DQE of the device decreases less rapidly with the increasing temperature. This is translated into the laser being more thermally stable. The characteristic temperature T_0 is determined by plotting the threshold current density J_{th} versus the laser device temperature on a logarithmic scale and then measuring the slope of the linear fit line, as shown in Fig. 10.

The inverse of the slope of the linear fit to this set of data points is the characteristic temperature T_0 value. InGaN TQW lasers showed strong temperature dependence of J_{th} as shown in Fig. 10 in the range of $280-340$ K with the cavity length L of 800 μm. Our work implies that with the MQW structure, T_0 value of InGaN lasers could be greatly improved. We observed that InGaN SQW and TQW exhibit stronger temperature dependence than that of InGaN DQW lasers. This temperature dependence is determined by non-radiative recombination, current overflow, and other thermally activated processes. Additionally, the inhomogeneous carrier distribution ovserved in the quantum wells, is another important parameter that determines the reduction in the DQE value with the increase in temperature. We believe that there is still a large field for further optimization of the thermal stability in nitride devices since the highest reported T_0 is around 235 K[14].

In conclusion, we have found that the problem of inhomogeneous carrier distribution in InGaN LD structures deteriorates with the increase of quantum well number for the spectral range under study. The inhomogeneous carrier distributions in the quantum wells play an important role in the laser performance. The lowest threshold current, higher external quantum efficiency and characteristic temperature are obtained when the number of InGaN well layers is two at our laser emission wavelength of 415 nm. The effects of device temperature on the laser threshold current, external DQE, and output wavelength exhibit significant variation in these parameter values.

The financial supports from Universiti Sains Malaysia, Ministry of Science Technology and Innovation (MOSTI) and Ministry of Higher Education are gratefully acknowledged.

References

1. S. F. Chichibu, A. C. Abare, M. S. Minsky, S. Keller, S. B. Fleischer, J. E. Bowers, E. Hu, U. K. Mishra, L. A. Coldren, S. P. DenBaars, and T. Sota, Appl. Phys. Lett. **73,** 2006 (1998).

2. E. Berkowicz, D. Gershoni, G. Bahir, E. Lakin, D. Shilo, E. Zolotoyabko, A. C. Abare, S. P. Denbaars, and L. A. Coldren, Phys. Rev. B **61,** 10994 (2000).
3. Z. I. Kazi, T. Egawa, T. Jimbo, and M. Umeno, IEEE Photon. Technol. Lett. **11,** 1563 (1999).
4. T. Higashi, T. Yamamoto, S. Ogita, and M. Kobayashi, IEEE J. Sel. Top. Quantum Electron. **3,** 513 (1997).
5. J. Piprek, P. Abraham, and J. E. Bowers, IEEE J. Sel. Top. Quantum Electron. **5,** 643 (1999).
6. K. Domen, R. Soejima, A. Kuramata, K. Horino, S. Kubota, and T. Tanahashi, Appl. Phys. Lett. **73,** 2775 (1998).
7. Integrated System Engineering (ISE TCAD) AG, Switzerland, http://www.synopsys.com (Feb. 25, 2008).
8. H. Y. Zhang, X. H. He, Y. H. Shih, M. Schurman, Z. C. Feng, and R. A. Stall, Opt. Lett. **21,** 1529 (1996).
9. R. K. Sink, "Cleaved-facet III-nitride laser diode" PhD Thesis (University of California at Santa Barbara, 2000).
10. D. Fritsch, H. Schmidt, and M. Grundmann, Phys. Rev. B **67,** 235205 (2003).
11. J. Wu, W. Walukiewicz, K. M. Yu, J. W. Ager III, E. E. Haller, H. Lu, and W. J. Schaff, Appl. Phys. Lett. **80,** 4741 (2002).
12. S. Nukamura, M. Senoh, S. Nagahama, N. Iwasa, T. Yamada, T. Matsushita, H. Kiyoku, Y. Sugimoto, T. Kozaki, H. Umemoto, M. Sano, and K. Chocho, Jpn. J. Appl. Phys. **37,** L1020 (1998).
13. S. M. Thahab, H. A. Hassan, and Z. Hassan, Opt. Express **15,** 2380 (2007).
14. T. Mukai, S. Nagahama, T. Yanamoto, and M. Sano, Phys. Stat. Sol. a **192,** 261 (2002).